Spectroscopic studies and crystal-field analyses of Am^{3+} and Eu^{3+} in the cubic-symmetry site of ThO_2

S. Hubert and P. Thouvenot
Laboratoire de Radiochimie, Institut de Physique Nucléaire, Boîte Postale No. 1, 91406 Orsay, France

N. Edelstein
Lawrence Berkeley Laboratory, Chemical Sciences Division, University of California, Berkeley, California 94720
(Received 1 February 1993)

Fluorescence and excitation spectra of Am^{3+} diluted in ThO_2 are reported at room and liquid-helium temperatures along with fluorescence data for Eu^{3+} diluted in ThO_2. The Eu^{3+} data can be assigned primarily to magnetic-dipole transitions, but the Am^{3+} data appear to be primarily phonon-assisted electric-dipole transitions. Earlier electron-paramagnetic-resonance (EPR) data on Pu^{3+} diluted in ThO_2 have set limits on the possible ratios of the crystal-field parameters B_0^4/B_0^6 for this system. Assuming the same ratio should hold for Am^{3+}-ThO_2, the observed transitions were assigned and the values for the crystal-field parameters $B_0^4=-6731\ cm^{-1}$, $B_0^6=714\ cm^{-1}$ were obtained. The B_0^4 value is the same order of magnitude as found earlier in inelastic-neutron-scattering experiments for UO_2 and NpO_2, but B_0^6 for Am^{3+}-ThO_2 is much smaller than determined in the neutron experiments.

I. INTRODUCTION

Few detailed analyses of the optical spectra of trivalent americium in highly symmetric cationic sites have been published. The most complete analysis has been given by Carnall[1] for Am^{3+} in $LaCl_3$ and $AmCl_3$[2,3] where the Am^{3+} ion is at a site of D_{3h} symmetry. By fitting the absorption and fluorescence data to a phenomenological Hamiltonian, Carnall found very good agreement between the calculated and experimental energy levels. Chudnovskaya *et al.*[4,5] have reported the absorption and fluorescence spectra of Am^{3+} in $Cs_2NaLnCl_6$, where Am^{3+} is at an O_h-symmetry site. However, the crystal-field analysis was carried out only for the absorption and luminescence spectra in the ground-term (^7F) region. In this paper we present the experimental results and an analysis of the fluorescence and excitation spectra of the isoelectronic ions Am^{3+} ($5f^6$) and Eu^{3+} ($4f^6$) diluted in powdered samples of ThO_2.

Thorium dioxide is an interesting host matrix for a variety of reasons. It is easy to synthesize as a powder, it crystallizes in the face-centered-cubic structure described by the O_h^5 space group (fluorite structure), and it is the first and simplest member (no $5f$ electrons) of the actinide dioxide series. Optical studies have been published on tetravalent actinides diluted in ThO_2.[6,7] Electron-paramagnetic-resonance (EPR) studies of Pu^{3+} in ThO_2 (Ref. 8) plus optical studies of trivalent f^n ions[9–13] in ThO_2 suggest that the local symmetry remains cubic and thus make this matrix attractive for further work. Preliminary results on the luminescence properties of Am^{3+} ($5f^6$) and Eu^{3+} ($4f^6$) (Refs. 9 and 10) have confirmed that, at least for diluted samples, both ions are substituted into the cationic site and retain cubic symmetry. Since trivalent ions replace a 4+ ion host, the charge compensation appears to migrate far away from the dopant ions.

The heavier actinide dioxides (UO_2, NpO_2, and PuO_2) have been the subjects of numerous studies.[14–18] One of the major questions about these materials is the interaction of the $5f$ electrons of the actinide ion with their neighbors. The traditional way of describing such a system is in terms of a single-ion crystal-field Hamiltonian which, for an f^n ion in O_h symmetry, requires two crystal-field parameters. Recently, inelastic neutron scattering has been used to determine the crystal-field energy levels of the ground multiplets of UO_2, NpO_2, and PuO_2, and the data were analyzed in terms of the crystal-field model.[15,17,18] Also, Goodman has presented local-density molecular-orbital calculations which give estimates of the crystal-field parameters in the actinide dioxides.[14]

In this paper the crystal-field parameters for Am^{3+} in ThO_2 are derived from the analysis of the optical spectra. These parameters together with the previously reported EPR data of Pu^{3+} and Am^{4+} in ThO_2 and CeO_2 provide an estimate of the crystal field for Am^{4+} in CeO_2. CeO_2 is isostructural with the actinide dioxides and has a lattice parameter between NpO_2 and PuO_2. These results will be discussed and compared with earlier measurements.

II. EXPERIMENTAL PROCEDURE

The ThO_2 samples doped with Am^{3+} (5×10^{-2} at. %) and Eu^{3+} (0.1 at. %) were synthesized as powders according to the method described earlier.[9] Although Kolbe *et al.*[8] had measured the EPR spectrum of Am^{4+} in single crystals of Am-ThO_2, no evidence of tetravalent americium could be found optically in our samples. If Am^{4+} exists in our samples, it might be at a much smaller concentration than for Am^{3+}. The calcination temperature used for synthesizing the Am-ThO_2 powder

(850 °C) is lower than the single-crystal synthesis temperature (1350 °C).[8] The synthesis procedure could influence the final oxidation state of the Am ion.

Fluorescence spectra were recorded between room and liquid-helium temperatures and analyzed with a 1-m JOBIN-YVON monochromator with a dispersion of 8 Å/mm. Fluorescence between 400 and 850 nm was detected by a photomultiplier (R 636 Hamamatsu), while fluorescence from 800 to 2400 nm was detected by a PbS photodiode. This experimental setup was controlled by a PC. The sample was placed in a liquid-helium optical cryostat (OXFORD Instruments) with a regulated, heated-gas system allowing the temperature to be varied between 10 and 300 K. A SOPRA nitrogen laser (pulse length 7 ns) followed by a LAMBDA-PHYSIK dye laser (pulse length 7 ns and linewidth 0.1 cm^{-1}) was used as the excitation source for the fluorescence and excitation spectra reported in this paper.

III. THEORY AND SYMMETRY CONSIDERATIONS

The crystal structure of thorium dioxide has each Th^{4+} ion at the center of a cube of oxygen ions, and each oxygen ion has around it a tetrahedron of thorium ions.[19] The ThO_2 structure is isomorphic with the CaF_2 structure and has space-group symmetry O_h^5. However, in the far-infrared (FIR) spectrum of our pure powdered sample, a slight distortion was observed.[10] Weak shoulders appeared in the spectrum around 96 and 275 cm^{-1}, the FIR-active mode at 356 cm^{-1} was the most intense, but the Raman-active mode at 456 cm^{-1} (Refs. 20 and 21) (inactive in FIR) was observed as well. Nevertheless, several experimental observations[10,13] suggest that, like tetravalent actinides,[6] the trivalent ions Eu^{3+} and Am^{3+} diluted in the matrix are substituted into the cationic site and keep the eightfold cubic symmetry. This means that for diluted systems using our synthesis procedure, the charge compensation vacancies migrate far away from the dopant ions.

In the case of a structure with an inversion center, the f-f electric-dipole transitions are forbidden by the selection rules, while the f-f magnetic-dipole transitions ($\Delta J=1$) are allowed. Thus the excitation and fluorescence spectra have a predominantly vibronic character. In our data the normal-mode frequencies appeared to be about the same for coupling to the ground state as to the excited electronic states. The electronic energy levels deduced from the excited-state vibronic structure were fit by simultaneous diagonalization of the free-ion and crystal-field Hamiltonians H_{FI} and H_{CF}, where

$$H_{FI}=\sum_{k=0,2,4,6} F^k(nf,nf)f_k+\zeta_f\alpha_{s.o.}+\alpha L(L+1)+\beta G(G_2)+\gamma(R_7)+\sum_{\substack{k=2,8\\k\neq 5}} T^k t_k+\sum_{k=0,2,4} M^k m_k+\sum_{k=2,4,6} P^k p_k$$

and

$$H_{CF}=B_0^4[C_0^4+(\tfrac{5}{14})^{1/2}(C_{-4}^4+C_4^4)]+B_0^6[C_0^6-(\tfrac{7}{2})^{1/2}(C_{-4}^6+C_4^6)]\,.$$

The $F^k(nf,nf)$'s and ζ_f above represent the radial parts of the electrostatic and spin-orbit interactions, respectively, between f electrons, while f_k and $\alpha_{s.o.}$ are angular parts of these interactions. The parameters α,β,γ are associated with the two-body effective operators of the configuration interaction, and the T_s^k are the corresponding parameters of the three-body configuration interaction operators. The M^k parameters represent the spin-spin and spin-other-orbit interactions, while the P^k parameters arise from electrostatic-spin-orbit interactions with higher configurations. The crystal-field interaction for O_h symmetry is parametrized by B_0^4 and B_0^6, and the angular operators $C_q^{(k)}$ are the usual Racah tensors.[22]

Crystal-field parameters for trivalent actinides substituted for Th^{4+} ions in ThO_2 have not been evaluated. However, EPR measurements on Pu^{3+}-ThO_2 do set limits on the possible ratios of the parameters B_0^4/B_0^6. For Pu^{3+} in cubic symmetry, the Γ_7 ($J=\frac{5}{2}$) crystal-field state is the ground state. Higher-lying crystal-field states are relatively close in energy and are coupled into the ground state by the crystal field. The measured g value thus depends on the strength of the crystal field, and the relative strengths of the crystal field at the Pu^{3+} impurity site for

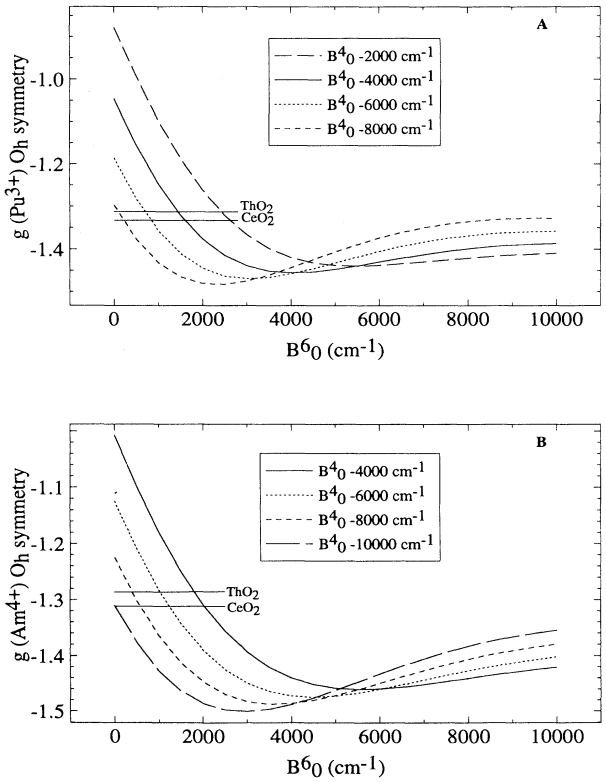

FIG. 1. Calculated g values as a function of the crystal-field parameters for O_h symmetry: (a) ground state of Pu^{3+}-ThO_2 and (b) ground state of Am^{4+}-ThO_2 or Am^{4+}-CeO_2. The horizontal lines represent the measured g values.

a number of different cubic host crystals have been determined by this method.[23,24]

The measured g value for the ground Γ_7 ($J=\frac{5}{2}$) state of Pu^{3+}-ThO_2 is $|g|=1.3124(5)$. Since Pu and Am are nearest neighbors in the periodic table, we expect the crystal field at a Th^{4+} cubic site to be very similar. In order to limit the possible values of the crystal-field parameters, we assume that, at least in the initial fitting procedures, the values of the Am^{3+} crystal-field parameters for Am^{3+}-ThO_2 must also fit the measured g value for Pu^{3+}-ThO_2. Some ranges of values for the crystal-field parameters which give the measured g value for Pu^{3+} are shown in Fig. 1(a). The calculated values were obtained by using all free-ion energy levels below $\sim 20\,000$ cm^{-1} to calculate crystal-field matrix elements and then diagonalizing the resulting matrices following the procedures of Crosswhite and Crosswhite.[25] The g values of the ground state were calculated from the resultant eigenvectors.

The energy levels for Am^{3+}-ThO_2 were obtained in a similar way. The free-ion energy levels up to 30 000 cm^{-1} were determined using the free-ion parameters found by Carnall for Am^{3+}-$LaCl_3$. The crystal-field matrix elements were calculated with these free-ion eigenvectors, and these matrices were used to fit the experimental electronic levels.

IV. EXPERIMENTAL RESULTS AND ANALYSIS OF THE SPECTRA

All optical spectra reported in this paper were obtained on powders. All transitions and/or states will be described by referring to either the free-ion J states and/or the O_h group labels ($\Gamma_1,\Gamma_2,\Gamma_3,\Gamma_4,\Gamma_5$) for an f^n ion, where n is an even number. In this notation, Γ_1 and Γ_2 are singlets, Γ_3 is a doublet, and Γ_4 and Γ_5 are triplets.[26] All crystal-field states from the various J multiplets may be classified by these symmetry labels. The lowest-energy Γ_N state ($N=1-5$) will be numbered 1, the second lowest Γ_N state 2, etc. Only crystal-field states of the same symmetry (but of different J) may be mixed by the crystal-field potential, and so the Γ_N labels remain as good quantum numbers. Since J mixing does occur and some levels contain more than one J component, the Am^{3+} states will be labeled by the largest J component and a prime will be added, i.e., J'.

A. Fluorescence spectra

The luminescence spectrum of Am^{3+}-ThO_2 in the visible has been already reported elsewhere,[9,10] and the observed lines primarily were assigned to transitions originating from the ${}^5D_{1'}$ state to the ground ${}^7F_0$ and low-lying ${}^7F_{2'}$ levels in the regions 570–620 nm (${}^5D_{1'}\rightarrow{}^7F_{0'}$), 650–750 nm (${}^5D_{1'}\rightarrow{}^7F_{1'}$), and 800–850 nm (${}^5D_{1'}\rightarrow{}^7F_{2'}$) [Fig. 2(a)].[27] A weak group of lines was observed also in the range 520–560 nm corresponding to ${}^5L_{6'}\rightarrow{}^7F_{0'}$ transitions. Among these groups the most intense transitions correspond to the ${}^5D_{1'}\rightarrow{}^7F_{1'}$ and ${}^5D_{1'}\rightarrow{}^7F_{2'}$. In the infrared spectrum [Fig. 2(b)], only two groups of lines appear. The two lines at 8202 and 9350 Å are assigned to ${}^5D_{1'}\rightarrow{}^7F_{2'}$ transition, while the group of lines between

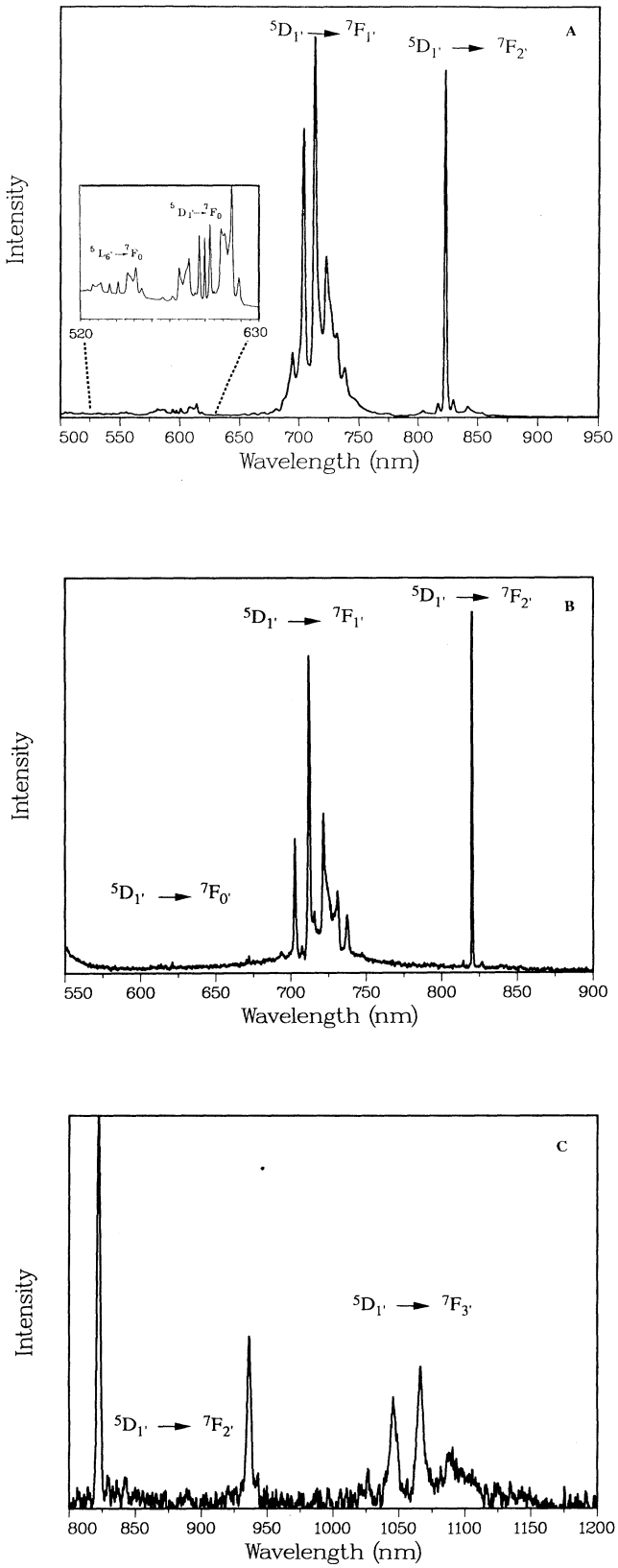

FIG. 2. Emission spectra of Am^{3+}-ThO_2: (a) visible region at room temperature, (b) visible region at 10 K, and (c) infrared region at room temperature.

1000 and 1150 nm is assigned as $^5D_{1'} \rightarrow {}^7F_{3'}$. The vibronic band structure for all the groups makes possible the identification of the purely electronic (zero-phonon) and phonon-assisted transitions in the luminescence spectrum. From the vibronic structure, the zero-phonon electric-dipole transitions $^5L_{6'} \rightarrow {}^7F_{0'}$, $^5D_{1'} \rightarrow {}^7F_{1'}$, and $^5D_{1'} \rightarrow {}^7F_{3'}$ were deduced and six Stark components $^7F_{1'}(\Gamma_4)$, $^7F_{2'}(\Gamma_5)$, $^7F_{2'}(\Gamma_3)$, $^7F_{3'}(\Gamma_4)$, $^5D_{1'}(\Gamma_4)$, and $^5L_{6'}(\Gamma_2)$ could be calculated respectively at 2637, 4583, 6079, 7294, 16 765, and 18 496 cm^{-1}. The assignment of transitions from the luminescence spectrum at low temperature is presented in Table I along with the frequencies belonging to the vibrations of the lattice. Note that the vibronic structure associated with most of the zero-phonon lines (allowed or forbidden) contains all the frequencies corresponding to the complete vibrational representation of the lattice.[10] The most intense zero-phonon lines observed in the spectrum are attributed to the magnetic-dipole transition $^5D_{1'} \rightarrow {}^7F_{2'}$. In contrast to the other transitions, they are accompanied by weak vibronic structure. In O_h symmetry the $^5D_{1'}$ level is not split by the crystal field; therefore, the energy difference between the narrow lines at 8202 and 9350 Å [see Fig. 2(b)] gives directly the splitting of the $^7F_{2'}$ level ($\Delta E = 1496$ cm^{-1}).

TABLE I. Zero-phonon and phonon-assisted transitions energies from the luminescence spectrum at low temperature [notation from Nielson and Koster (Ref. 27)].

Wavelength λ (Å)	Wave number ν (cm^{-1})$_{vac}$	Assignment[a]	ΔE
(5402)	(18 506)	$^5L_{6'} \rightarrow {}^7F_{0'}(3\Gamma_2 \rightarrow 1\Gamma_1)$	0
5429	18 414		93
5486	18 223		283
5540	18 045		461
5575	17 932		574
5929	16 861		93
5961	16 771	$^5D3_{1'} \rightarrow {}^7F_{0'}(7\Gamma_4 \rightarrow 1\Gamma_1)$	0
5995	16 676		92
6065	16 483		285
6091	16 413		355
6129	16 308		460
6173	16 195		573
7024	14 232		97
7072.5	14 135	$^5D3_{1'} \rightarrow {}^7F_{1'}(7\Gamma_4 \rightarrow 1\Gamma_4)$	0
7118	14 044		92
7214	13 857		274
7309	13 677		459
7373	13 559		575
8202	12 189	$^5D3_{1'} \rightarrow {}^7F_{2'}(7\Gamma_4 \rightarrow 1\Gamma_5)$	0
8269	12 089		99
8397	11 905		283
9350	10 692	$^5D3_{1'} \rightarrow {}^7F_{2'}(7\Gamma_4 \rightarrow 1\Gamma_3)$	0
10 249	9754		277
10 447	9569		93
(10 549)	(9477)	$^5D3_{1'} \rightarrow {}^7F_{3'}(7\Gamma_4 \rightarrow 2\Gamma_4)$	0
10 653	9384		93
10 877	9191		286
10 957	9124		353

[a]See Table IV for a tabulation of the Am^{3+} states.

TABLE II. Magnetic-dipole transitions energies of Eu^{3+}-ThO_2 from the emission spectrum at 10 K (Ref. 27).

Wavelength λ (Å)	Wave number ν (cm^{-1})$_{vac}$	Assignments[a]
5903	16 936	$^5D3_0 \rightarrow {}^7F_1$ ($4\Gamma_1 \rightarrow 1\Gamma_4$)
5680.5	17 600	$^5D3_1 \rightarrow {}^7F_2$ ($7\Gamma_4 \rightarrow 1\Gamma_3$)
5477.5	18 251	$^5D3_1 \rightarrow {}^7F_4$ ($7\Gamma_4 \rightarrow 1\Gamma_5$)
5258.5	19 012	$^5D3_1 \rightarrow {}^7F_0$ ($7\Gamma_4 \rightarrow 1\Gamma_1$)
5188	19 270	$^5D3_2 \rightarrow {}^7F_3$ ($5\Gamma_3 \rightarrow 1\Gamma_2$)[b]
5158	19 382	$^5D3_2 \rightarrow {}^7F_3$ ($5\Gamma_3 \rightarrow 2\Gamma_5$)
5121.5	19 520	$^5D3_2 \rightarrow {}^7F_3$ ($5\Gamma_3 \rightarrow 2\Gamma_4$)
4751	21 042	$^5D3_3 \rightarrow {}^7F_4$ ($3\Gamma_2 \rightarrow 3\Gamma_5$)
4737.5	21 102	$^5D3_2 \rightarrow {}^7F_1$ ($5\Gamma_3 \rightarrow 1\Gamma_4$)
4719	21 185	$^5L_6 \rightarrow {}^7F_4$ ($4\Gamma_2 \rightarrow 4\Gamma_5$)
4678.5	21 368	$^5D3_3 \rightarrow {}^7F_4$ ($8\Gamma_5 \rightarrow 2\Gamma_3$)
4663.5	21 437	$^5D3_3 \rightarrow {}^7F_4$ ($8\Gamma_4 \rightarrow 2\Gamma_3$)
4517.5	22 130	$^5L_6 \rightarrow {}^7F_4$ ($10\Gamma_5 \rightarrow 2\Gamma_3$)
4466.5	22 383	$^5D3_3 \rightarrow {}^7F_3$ ($8\Gamma_4 \rightarrow 2\Gamma_5$)

[a]See Table V for a tabulation of the Eu^{3+} states.
[b]Not an allowed magnetic-dipole transition.

By comparison with the Am^{3+}, the luminescence spectrum of the isoelectronic lanthanide ion Eu^{3+} is straightforward.[10] The magnetic-dipole transition $^5D_0 \rightarrow {}^7F_1$ at 5903 Å is the most intense emission line observed in the spectrum,[10] and other narrow, weaker lines are attributed as well to magnetic-dipole transitions ($\Delta J = 1$) as shown in Table II. All but one of the observed Eu^{3+} transitions can be assigned as magnetic-dipole transitions; phonon-assisted transitions are not observed. For Eu^{3+} the splitting of $^7F_2$ level is 651 cm^{-1}, about half the splitting of Am^{3+}-ThO_2.

B. Excitation spectra

For Am^{3+}-ThO_2, excitation spectra at room temperature and 4.2 K were obtained in the visible region by

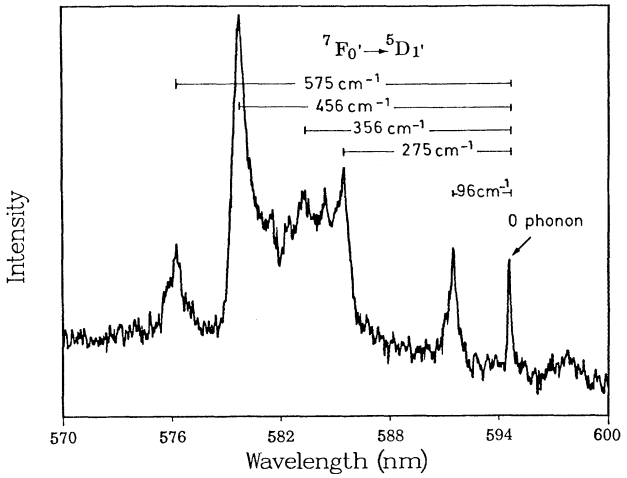

FIG. 3. Am^{3+}-ThO_2 excitation spectrum at room temperature, the $^7F_{0'} \rightarrow {}^5D_{1'}$ transition (Ref. 27).

monitoring the strongest emission line at 7118 or 8202 Å. Several dyes (BBQ, Coumarine 440, 460, 503, Rhod. 590) were used to obtain these spectra. Figure 3 shows the excitation spectrum obtained at room temperature in the $^5D_{1'}$ region using Rhodamine 590. As in the fluorescence spectrum, we clearly can assign the zero-phonon line $^7F_{0'} \rightarrow {}^5D_{1'}$ at 5963 Å (16 765 cm^{-1}), which is accompanied by the characteristic vibronic structure on the higher-energy side. The oscillator strength of this transition is very weak[28,29] and has only been observed once before in octahedral symmetry.[4,5] We observe this transition at room temperature in the excitation spectrum and its inverse in the emission spectrum. Unfortunately, at low temperature (below 50 K), the fluorescence intensity is bleached by traps which may be caused by defects due to oxygen vacancies, and so clean excitation spectrum

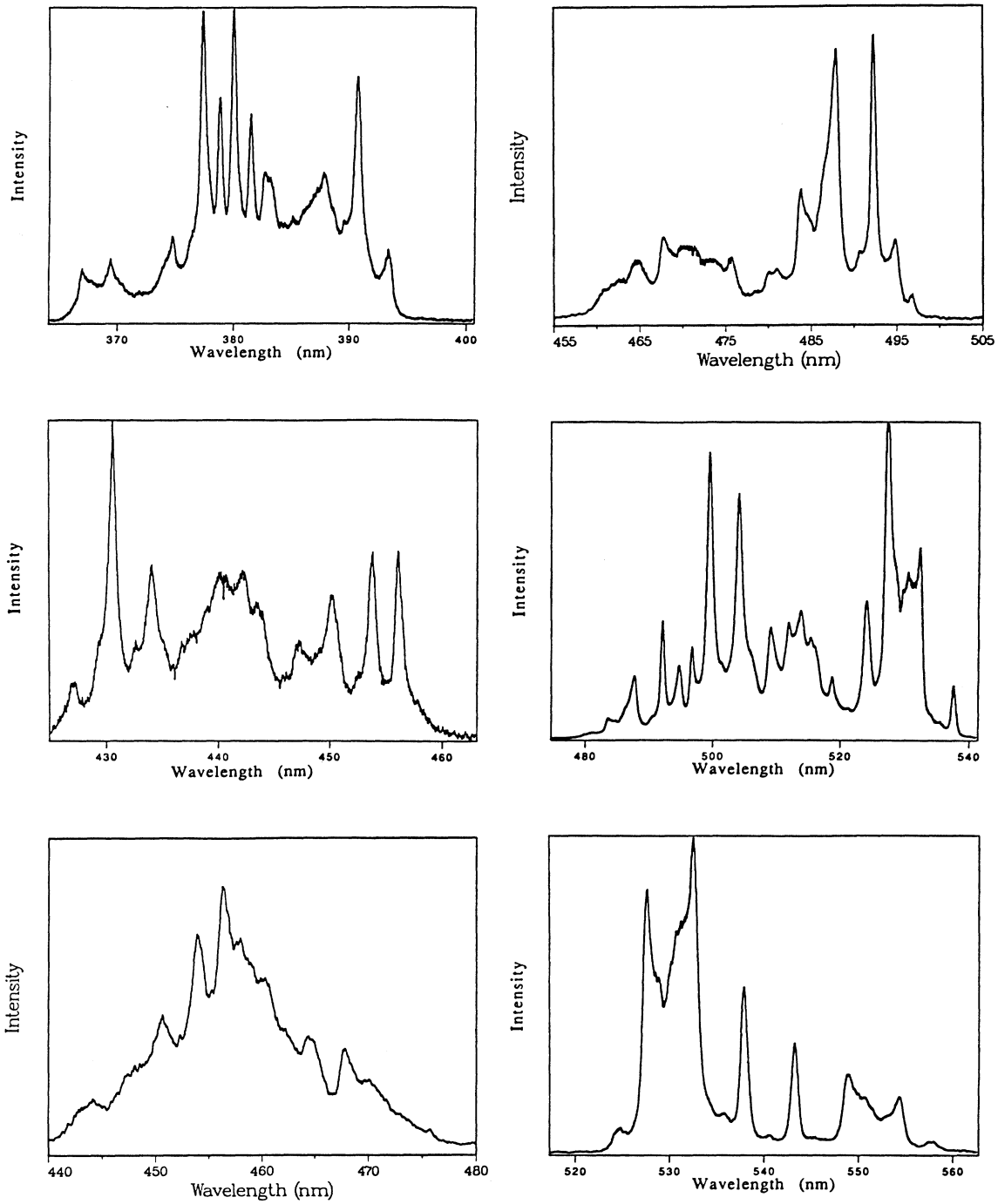

FIG. 4. Excitation spectra of Am^{3+}-ThO_2 at 10 K. The fluorescence is measured at 712 nm.

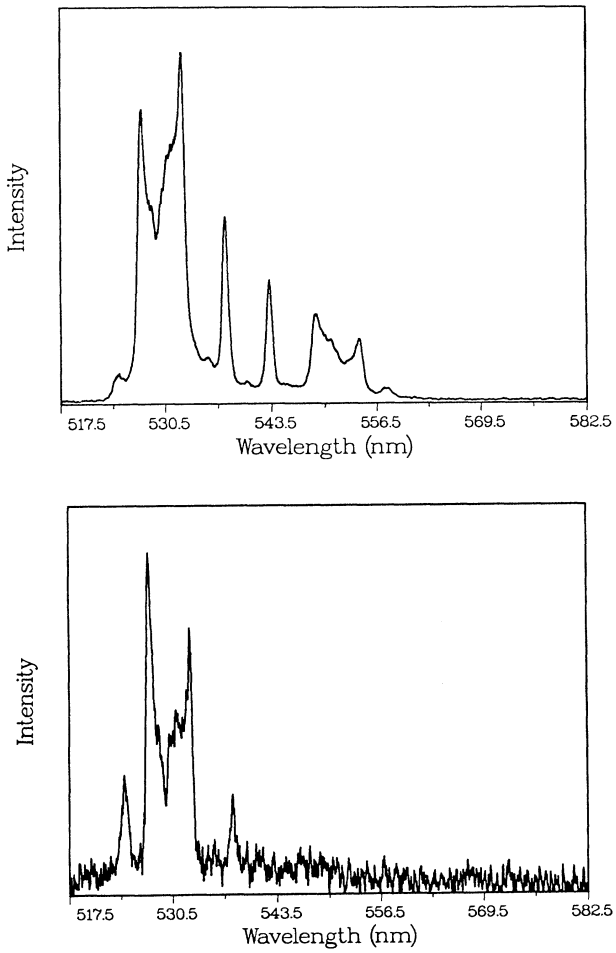

FIG. 5. Excitation spectra of the $^7F_0 \rightarrow {}^5L_6$ transition at room temperature and 4.2 K.

could not be obtained in this wavelength region. Excitation spectra were recorded at room and liquid-helium temperatures in the following regions: 365–400, 425–465, 440–480, 460–500, 475–555, and 517–582 nm. The excitation spectra at low temperature are shown in Fig. 4. Vibronic features are clearly observed in the $^5D_{1'}$ region and can be recognized in other spectral regions where the excited states are rather isolated. Such is the case for the lowest- and highest-energy components of $^5L_{6'}$ states between 515 and 560 nm and 480 and 490 nm, as well as in the region of the $^5D_{2'}$ and $^5G_{4'}$ levels between 440 and 480 nm. Among all the transitions observed in the excitation spectra, the only zero-phonon line which appears corresponds to the magnetic-dipole transition ($\Delta J = 1$) $^7F_0 \rightarrow {}^5D_{1'}$ at 5963 Å. Note, however, that for the lowest-energy component of the $^5L_{6'}$, the zero-phonon line centered between the two vibronic features (see Fig. 5) appears weakly at room temperature. When the temperature is decreased, the low-energy side of the vibronic structure disappears as expected.

From an analysis of the vibronic structure, the energies of some zero-phonon lines were identified. Table III lists the energies of 13 Stark components and the vibronic lines associated with them. Similar to the transitions observed in the fluorescence spectrum (Table II), the vibronic structure associated with the electronic transitions contains primarily the same phonon frequencies 96, 276, 456, and 575 cm^{-1} observed in the far-infrared spectrum.[10] Assignments of the Am^{3+}-ThO_2 levels are derived from the fluorescence and excitation measurements.

In contrast with Am^{3+}, the excitation spectrum of Eu^{3+} in the cubic site is very simple. No phonon-assisted transitions are observed, and only one narrow line at 5255 Å corresponding to the magnetic-dipole transition $^7F_0 \rightarrow {}^5D_1$ is observed at low temperature (Fig. 6).

V. DISCUSSION

The levels were fit by simultaneous diagonalization of the free-ion and crystal-field Hamiltonians as given earlier. For Am^{3+}-ThO_2 the Am^{3+}-$LaCl_3$ free-ion parameters were used as initial guesses along with a series of values of B_0^4 and B_0^6 which were chosen to give the experimental ground-state g value for Pu^{3+}-ThO_2. Initially, the crystal-field parameters were held fixed and only F^2, F^4, F^6, and ζ were varied. After the "best" values of B_0^4 and B_0^6 were determined, further high-energy levels were assigned, and the above free-ion and crystal-field parame-

TABLE III. Energies of zero-phonon and phonon-assisted lines from excitation spectra at low temperature.

Wavelength λ (Å)	Wave numbers ν (cm^{-1}) in vacuum	Δν (phonons)	Wavelength λ (Å)	Wave numbers ν (cm^{-1}) in vacuum	Δν (phonons)
5963	16 765	0	4776	20 932	0
5929	16 861	96	4754	21 029	97
5865	17 045	280	4715	21 203	271
5805	17 221	456	4674	21 389	457
5765	17 341	576	4649	21 504	572
5405	18 496	0	4661	21 448	0
5378	18 589	93	4640	21 546	98
5325	18 774	278	4602	21 724	276
5275	18 952	456	4563	21 909	461
5242	19 072	576	4540	22 020	572

TABLE III. (*Continued*).

Wavelength λ (Å)	Wave numbers ν (cm^{-1}) in vacuum	Δν (phonons)	Wavelength λ (Å)	Wave numbers ν (cm^{-1}) in vacuum	Δν (phonons)
5214	19 174	0	4493	22 251	0
5188	19 270	96	4474	22 345	94
5139	19 453	279	4437	22 531	280
5119	19 530	356	4404	22 702	451
5091	19 637	465	4379	22 830	579
5063	19 746	572			
			4396	22 740	0
5116	19 541	0	4377	22 840	100
5091	19 637	96	4344	23 014	274
5045	19 817	276	4309	23 201	461
5029	19 879	333	4361	22 924	0
4999	19 998	449	4344	23 014	90
4971	20 111	570	4308	23 206	282
			4295	23 276	356
5060	19 757	0	4275	23 385	461
5036	19 851	94			
4990	20 034	277	3947	25 328	0
4971	20 111	354	3922	25 425	97
4944	20 221	464	3904	25 607	279
4916	20 336	579	3877	25 786	458
			3861	25 893	565
4950	20 196	0	3840	26 034	0
4927	20 291	95	3826	26 126	92
4883	20 473	277	3800	26 308	274
4874	20 515	319	3788	26 392	358
4837	20 668	464	3773	26 497	463
4815	20 763	567	3762	26 574	540

ters were varied simultaneously. In the final iterations, the parameter α was varied also. For Eu^{3+}-ThO_2, the free-ion parameters (except for ζ) were fixed at the values obtained from analysis of the fluorescence data of Eu^{3+}-$LuPO_4$;[30] ζ and the crystal-field parameters B_0^4 and B_0^6 were allowed to vary. The results of the fits and the final assignments of the experimental levels are given in Table IV for Am^{3+}-ThO_2 and in Table V for Eu^{3+}-ThO_2. The parameters are given in Table VI. O_h-symmetry labels were assigned on the basis of the calculated energy levels and wave functions.

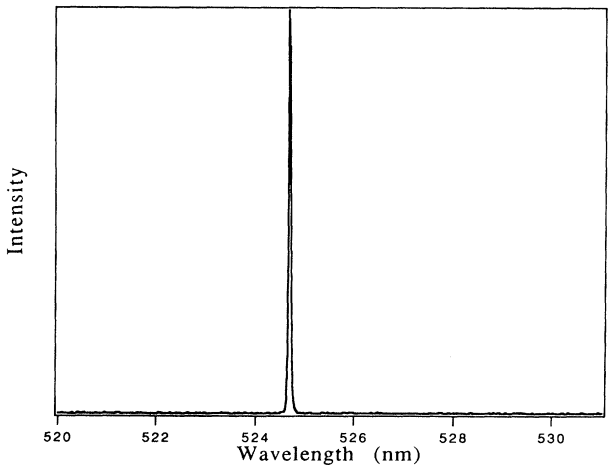

FIG. 6. Excitation spectrum of Eu^{3+}-ThO_2 at 10 K.

As expected, the crystal-field parameters of Am^{3+}-ThO_2 are appreciably larger than for Eu^{3+}-ThO_2. Although we have observed only a very limited number of Am^{3+} multiplets, the free-ion parameters F^2, F^4, F^6, and ζ appear to be smaller than those found by Carnall for Am^{3+}-$LaCl_3$.[1] The value of the parameter α is larger than that used by Carnall, but the large error associated with this parameter in our work suggests this comparison is not meaningful. The values of the crystal-field parameters seem reasonable in that we are able to get a good fit for Am^{3+}-ThO_2 with crystal-field parameters which also give reasonable agreement with the measured g value for Pu^{3+}-ThO_2.

The results for Am^{3+}-ThO_2 allow a reexamination of the EPR data for Pu^{3+}-ThO_2, Am^{4+}-ThO_2, and Am^{4+}-CeO_2. We expect the crystal-field splittings for the tetravalent ion Am^{4+} to be larger than for the isoelectronic ion Pu^{3+}. In addition, if we compare the crystal fields for Am^{4+} in the host crystal ThO_2 ($a_0=5.597$ Å) and CeO_2 ($a_0=5.41$ Å), we would expect a larger crystal field in CeO_2 than in ThO_2 because of the larger lattice constant

in ThO_2.[31,32] This is exactly what is observed in the EPR spectra of Am^{4+}-ThO_2 and Am^{4+}-CeO_2 where the ground-state g value of Am^{4+} is larger in CeO_2 (absolute magnitude) due to increased mixing of higher-energy states by the larger crystal field. The calculated g values of Am^{4+} for various ranges of B_0^4 and B_0^6 are shown in Fig. 1(b).

We assume that the minimum value of B_0^4 for Am^{4+} in ThO_2 or CeO_2 is equal to that found for Am^{3+} in ThO_2. From Fig. 1(b) this assumption would put the value of B_0^6 for Am^{4+}-ThO_2 at ~ 800 cm^{-1}. Increasing the value of B_0^4 decreases B_0^6. If we make the same assumption for Am^{4+}-CeO_2, we get the values of $B_0^4 \cong -6700$ cm^{-1} and $B_0^6 \cong 1000$ cm^{-1}. Again, as B_0^4 get larger, B_0^6 must decrease in order to get the observed g value.

Now the lattice parameter of CeO_2 is between that of NpO_2 ($a_0 = 5.425$ Å) and PuO_2 ($a_0 = 5.396$ Å).[31] From the inelastic-neutron-scattering data for UO_2, the values of $B_0^4 = -7937$ cm^{-1} and $B_0^6 = 3420$ cm^{-1} were obtained.[18] The value of B_0^4 found in the neutron-scattering data is within 20% of the value we have obtained with Am^{3+} as a probe of the crystal field of ThO_2, but the B_0^6 found for UO_2 is inconsistent with the optical and EPR data of Am^{3+}-ThO_2, Pu^{3+}-ThO_2, and Am^{4+}-ThO_2,CeO_2.

UO_2 is a magnetic material, and the U^{4+} ion has a greater radial extent than Am^{4+}. Our experiments use a paramagnetic probe in a diamagnetic host which is isostructural with UO_2. Covalency effects in UO_2 could play a role which might affect our arguments about the magnitudes of the crystal-field parameters. However, the good agreement found for the UO_2 inelastic-neutron-scattering value of B_0^4 with our Am^{3+} B_0^4 value suggests the comparsion is valid. Our results also disagree with the magnitude of the crystal field obtained by Goodman in his calculations,[14] where he has found values of B_0^4 and B_0^6 of the same magnitude (but opposite sign) for UO_2, PuO_2, and CmO_2.

The crystal-field strength parameter N_v' (Ref. 33) provides a useful means for comparing crystal-field effects on

TABLE IV. Calculated and experimental energy levels for Am^{3+}-ThO_2 [notation from Nielson and Koster (Ref. 27)].

Level	Largest S-L-J Comp.	Calc. energy	Expt. energy	$\Delta(E_{exp}-E_{calc})$	Level	Largest S-L-J Comp.	Calc. energy	Expt. energy	$\Delta(E_{exp}-E_{calc})$
$1\Gamma_1$	$^7F_0$	4.2	0	−4.2	$9\Gamma_4$	$^5G1_3$	22 019.5		
$1\Gamma_4$	$^7F_1$	2655.6	2637	−18.6	$12\Gamma_5$	$^5H2_4$	22 266.2	22 251	−15.2
$1\Gamma_5$	$^7F_2$	4559.3	4583	23.7	$10\Gamma_4$	$^5H2_5$	22 311.0		
$1\Gamma_3$	$^7F_2$	6053.8	6079	25.2	$8\Gamma_3$	$^5H2_5$	22 336.7		
$2\Gamma_4$	$^7F_3$	7318.4	7294	−24.4	$11\Gamma_4$	$^5H2_5$	22 664.8		
$2\Gamma_5$	$^7F_3$	7703.9			$13\Gamma_5$	$^5L_7$	22 893.1		
$1\Gamma_2$	$^7F_3$	7960.3			$12\Gamma_4$	$^5L_7$	22 899.1		
$2\Gamma_1$	$^7F_4$	8225.1			$6\Gamma_1$	$^5H2_4$	22 928.5	22 924	−4.5
$3\Gamma_4$	$^7F_4$	9230.6			$5\Gamma_2$	$^5L_7$	22 952.2		
$2\Gamma_3$	$^7F_4$	9645.6			$9\Gamma_3$	$^5H2_4$	23 180.9		
$3\Gamma_5$	$^7F_4$	10 288.4			$13\Gamma_4$	$^5H2_5$	23 212.1		
$4\Gamma_5$	$^7F_5$	10 511.5			$14\Gamma_5$	$^5L_6$	23 320.1		
$4\Gamma_4$	$^7F_5$	10 734.8			$15\Gamma_5$	$^5L_7$	23 441.5		
$3\Gamma_3$	$^7F_5$	11 686.6			$10\Gamma_3$	$^5H2_4$	23 564.3		
$5\Gamma_4$	$^7F_5$	11 757.3			$16\Gamma_5$	$^5D3_3$	23 999.8		
$3\Gamma_1$	$^7F_0$	12 006.9			$6\Gamma_2$	$^5D3_3$	24 025.5		
$4\Gamma_1$	$^7F_6$	12 381.7			$14\Gamma_4$	$^5L_7$	24 055.4		
$6\Gamma_4$	$^7F_6$	12 579.8			$17\Gamma_5$	$^5L_6$	24 513.1		
$5\Gamma_5$	$^7F_6$	12 730.8			$11\Gamma_3$	$^5L_6$	24 606.9		
$2\Gamma_2$	$^7F_6$	12 822.0			$15\Gamma_4$	$^5D3_3$	24 663.4		
$4\Gamma_3$	$^7F_6$	13 035.6			$18\Gamma_5$	$^5L_6$	24 922.4		
$6\Gamma_5$	$^7F_6$	13 046.7			$7\Gamma_1$	$^5L_8$	24 973.0		
$7\Gamma_4$	$^5D3_1$	16 767.3	16 765	−2.4	$16\Gamma_4$	$^5L_6$	24 982.8		
$3\Gamma_2$	$^5L_6$	18 537.1	18 496	−41.2	$12\Gamma_3$	$^5L_8$	25 100.1		
$7\Gamma_5$	$^5L_6$	18 635.6			$8\Gamma_1$	$^5L_6$	25 101.2		
$5\Gamma_3$	$^5L_6$	18 677.5			$17\Gamma_4$	$^5D3_3$	25 214.6		
$8\Gamma_5$	$^5L_6$	19 114.0	19 174	60.1	$7\Gamma_2$	$^5D3_3$	25 319.0	25 328	9.0
$8\Gamma_4$	$^5L_6$	19 470.7	19 541	70.3	$19\Gamma_5$	$^5G2_4$	25 493.9		
$5\Gamma_1$	$^5L_6$	19 831.6	19 757	−74.6	$18\Gamma_4$	$^5G2_5$	25 979.2		
$6\Gamma_3$	$^5D3_2$	20 195.9	20 196	0.1	$13\Gamma_3$	$^5G2_5$	26 027.3	26 034	6.7
$9\Gamma_5$	$^5G1_2$	20 907.7	20 932	24.3	$20\Gamma_5$	$^5G2_5$	26 087.8		
$4\Gamma_2$	$^5G1_3$	21 289.5			$14\Gamma_3$	$^5G3_2$	26 183.5		
$10\Gamma_5$	$^5D3_2$	21 366.4			$19\Gamma_4$	$^5L_8$	26 252.3		
$7\Gamma_3$	$^5G1_2$	21 482.4	21 448	−34.4	$9\Gamma_1$	$^5G2_4$	26 498.5		
$11\Gamma_5$	$^5G1_3$	21 747.6							

TABLE V. Calculated and experimental energy levels for Eu^{3+}-ThO_2 [notation from Nielson and Koster (Ref. 27)].

Level	Largest S-L-J comp.	Calc. energy	Expt. energy	$\Delta(E_{expt}-E_{calc})$
$1\Gamma_1$	$^7F_0$	−20.1	0	20.1
$1\Gamma_4$	$^7F_1$	325.6	310	−15.6
$1\Gamma_5$	$^7F_2$	748.0	763	15.0
$1\Gamma_3$	$^7F_2$	1383.5	1414	30.5
$2\Gamma_4$	$^7F_3$	1886.8	1893	6.2
$2\Gamma_5$	$^7F_3$	2059.0	2031	−28.0
$1\Gamma_2$	$^7F_3$	2164.1	2143	−21.1
$2\Gamma_1$	$^7F_4$	2492.1		
$3\Gamma_4$	$^7F_4$	2816.7	2830	13.3
$2\Gamma_3$	$^7F_4$	2986.6	2993	6.4
$3\Gamma_5$	$^7F_4$	3287.3	3300	12.7
$4\Gamma_5$	$^7F_5$	3749.0		
$4\Gamma_4$	$^7F_5$	3811.0		
$3\Gamma_3$	$^7F_5$	4208.4		
$5\Gamma_4$	$^7F_5$	4244.3		
$3\Gamma_1$	$^7F_6$	4909.5		
$6\Gamma_4$	$^7F_6$	5022.7		
$5\Gamma_5$	$^7F_6$	5121.6		
$2\Gamma_2$	$^7F_6$	5293.2		
$6\Gamma_5$	$^7F_6$	5372.7		
$4\Gamma_3$	$^7F_6$	5390.2		
$4\Gamma_1$	$^5D3_0$	17 245.2	17 245	−0.2
$7\Gamma_4$	$^5D3_1$	19 020.3	19 012	−8.3
$5\Gamma_3$	$^5D3_2$	21 441.1		
$7\Gamma_5$	$^5D3_2$	21 551.7		
$3\Gamma_2$	$^5D3_3$	24 358.4	24 342	−16.4
$8\Gamma_5$	$^5D3_3$	24 370.5	24 361	−9.5
$8\Gamma_4$	$^5D3_3$	24 417.7	24 430	12.3
$6\Gamma_3$	$^5L_6$	24 429.5		
$9\Gamma_5$	$^5L_6$	24 450.3		
$4\Gamma_2$	$^5L_6$	24 494.5	24 485	−9.5
$10\Gamma_5$	$^5L_6$	25 132.8	25 123	−9.8
$9\Gamma_4$	$^5L_6$	25 240.6		
$5\Gamma_1$	$^5L_6$	25 377.0		

a series of f^n ions in the same matrix or the effects of different matrices with the same ion. Following Auzel and Malta, N_v' is defined as follows:

$$N_v' = \left[\sum_{k,q} (B_q^k)^2 \Big/ 2k+1\right]^{1/2} .$$

Values of N_v' for trivalent actinide ($5f^N$) ions with their counterpart ($4f^N$) lanthanide ions in different host matrices are given in Table VII.

TABLE VI. Spectroscopic parameters.[a]

Parameters (cm^{-1})	Eu^{3+}-ThO_2[b]	Am^{3+}-ThO_2[c]
F^2	[80335.2]	48 038.0(140.2)
F^4	[58953.9]	39 684.2(212.9)
F^6	[41636.6]	29 514.1(171.4)
ζ	1337.3(7.1)	2511.1(27.0)
α	[16.8]	33.2(8.6)
β	[−640]	[−660]
γ	[1750]	[1000]
T^2	[370]	[200]
T^3	[40]	[50]
T^4	[40]	[40]
T^6	[−330]	[−360]
T^7	[380]	[390]
T^8	[370]	[340]
M^0	[2.38]	[0.99]
M^2	[1.33]	[0.55]
M^4	[0.90]	[0.38]
P^2	[245]	[850]
P^4	[183.8]	[637.5]
P^6	[122.5]	[425]
B_0^4	−2780.2(32.2)	−6731.3(96.0)
B_0^6	266.0(26.3)	713.6(115.0)

[a]All parameters values in [ ] held fixed in the fitting procedure.
[b]17 experimental levels, rms deviation 18.0 cm^{-1}.
[c]17 experimental levels, rms deviation 47.3 cm^{-1}.

Comparison of the N_v' parameter with chloride coordination (D_{3h} for $LaCl_3$ and O_h for $AmCl_6^{3-}$) shows that the octahedral site provides a crystal field about twice as large as that of the D_{3h} site. The N_v' parameters for Am^{3+} or Eu^{3+} in ThO_2 when compared with these same ions in the elpasolite host are about twice as large. The larger crystal field found in ThO_2 is consistent with the shorter actinide-ligand distance [Th-O, 2.42 Å; Am-Cl, 2.54 Å]. We also report N_v' parameters for other $5f$ and $4f$ ion pairs (f^3 and f^5 configurations) in Table VII.[34,35] The strength of the crystal-field interaction is between 2 and 2.4 times larger for the trivalent actinide than for its counterpart lanthanide ion. This ratio can be used as a qualitative test of the validity of the crystal-field parameters. In ThO_2 we find the same ratio of $N_v'(5f^n)/N_v(4f^n)$ as in $LaCl_3$. Furthermore, this value is consistent with the splitting of the $^7F_2$ level found for Am^{3+} (1496 cm^{-1}), which is 2.3 times greater than for Eu^{3+} (646 cm^{-1}).

TABLE VII. N_v' parameters.

Ion	$Am^{3+}(Eu^3)$	$Am^{3+}(Eu^3)$	$Am^{3+}(Eu^3)$	$U^{3+}(Nd^{3+})$	$Pu^{3+}(Sm^3)$
Host	ThO_2	MCl_6^{3-}	$LaCl_3$	$LcCl_3$	$LaCl_3$
Symmetry	O_h	O_h	D_{3h}	D_{3h}	D_{3h}
Reference	This work	4	1,32	32,33	32,33
N_v' (cm^{-1})	2945(1212)	1165(618)	648(294)	605(302)	594(249)
$\frac{N_v'(5f^n)}{N_v'(4f^n)}$	2.4	1.9	2.2	2	2.4

VI. CONCLUSION

The fluorescence and excitation spectra of Am^{3+}-ThO_2 and the fluorescence spectra of Eu^{3+}-ThO_2 have been assigned. The crystal-field splittings of Am^{3+} in this crystal is approximately double that of its lanthanide analog, consistent with other actinide-lanthanide pairs. The fourth-order crystal-field parameter B_0^4 is of the same magnitude as found for UO_2 and NpO_2 by inelastic-neutron-scattering experiments, but the sixth-order parameter is appreciably smaller than that found in the neutron experiments.

ACKNOWLEDGMENT

This work was supported in part by the Office of Energy Research, Office of Basic Energy Sciences, Chemical Sciences Division of the U.S. Department of Energy under Contract No. DE-AC03-76SF00098.

[1]W. T. Carnall, J. Less-Common Met. **156**, 221 (1989).
[2]R. G. Pappalardo, W. T. Carnall, and P. R. Fields, J. Chem. Phys. **51**, 1182 (1969).
[3]J. G. Conway, J. Chem. Phys. **40**, 2504 (1964).
[4]G. P. Chudnovskaya, Yu. I. Gavrish, and Yu. A. Barbanel, Radiokhimiya **30**, 46 (1988).
[5]G. P. Chudnovskaya, R. B. Dushin, V. V. Kolin, and Yu. A. Barbanel, Radiokhimiya **27**, 545 (1985).
[6]J. B. Gruber and E. R. Menzel, J. Chem. Phys. **50**, 3772 (1969).
[7]Z. Gajek, M. P. LaHalle, J. C. Krupa, and J. Mulak, J. Less-Common Met. **139**, 351 (1988).
[8]W. Kolbe, N. Edelstein, C. B. Finch, and M. M. Abraham, Chem. Phys. **60**, 607 (1974).
[9]S. Hubert and P. Thouvenot, J. Alloys Compounds **180**, 193 (1992).
[10]S. Hubert and P. Thouvenot, J. Lumin. **54**, 103 (1992).
[11]R. C. Linares, J. Opt. Soc. Am. **56**, 107 (1966).
[12]M. Breysse and L. Faure, J. Lumin. **26**, 107 (1981).
[13]L. C. Porter and J. C. Wright, J. Lumin. **27**, 237 (1982).
[14]G. L. Goodman, J. Alloys Compounds **181**, 33 (1992).
[15]J. M. Fournier, A. Blaise, G. Amoretti, R. Caciuffo, J. Larroque, M. T. Hutchings, R. Osborn, and A. D. Taylor, Phys. Rev. B **43**, 1142 (1991).
[16]J. C. Krupa and Z. Gajek, Eur. J. Solid State Inorg. Chem. **28**, 143 (1991).
[17]S. Kern, C.-K. Loong, G. L. Goodman, B. Cort, and G. H. Lander, J. Phys. Condens. Matter **2**, 1933 (1990).
[18]G. Amoretti, A. Blaise, R. Caciuffo, J. M. Fournier, M. T. Hutchings, R. Osborn, and A. D. Taylor, Phys. Rev. B **40**, 1856 (1989).
[19]R. W. G. Wyckoff, *Crystal Structures,* 2nd ed. (Interscience, New York, 1963), Vol. 1.
[20]V. G. Keramidas and W. B. White, J. Chem. Phys. **59**, 156 (1973).
[21]G. M. Begun, R. G. Haire, W. R. Wilmarth, and J. R. Peterson, J. Less-Common Met. **162**, 129 (1990).
[22]W. T. Carnall, H. Crosswhite, H. M. Crosswhite, J. P. Hessler, N. M. Edelstein, J. G. Conway, G. V. Shalimoff, and R. Sarup, J. Chem. Phys. **72**, 5089 (1980).
[23]N. Edelstein, H. F. Mollet, W. C. Easley, and R. J. Mehlhorn, J. Chem. Phys. **51**, 3281 (1969).
[24]D. J. Lam and S.-K. Chan, Phys. Rev. B **6**, 307 (1972).
[25]H. M. Crosswhite and H. Crosswhite, J. Opt. Soc. Am. B **1**, 246 (1984).
[26]G. F. Koster, J. O. Dimmock, R. G. Wheeler, and H. Statz, *Properties of the Thirty-Two Point Groups* (MIT Press, Cambridge, MA, 1963).
[27]For an f^6 configuration, there are three ^5D states. In the notation of Nielson and Koster, the lowest ^5D state from which strong fluorescence occurs is labeled $^5D3$. In the text of this paper and in the figures, we use the notation ^5D for the $^5D3$ state. The tables list the states with the Nielson-Koster classification for the f^6 *LS* states. C. W. Nielson and G. F. Koster, *Spectroscopic Coefficients for the p^n, d^n, and f^n Configurations* (MIT Press, Cambridge, MA, 1963).
[28]W. T. Carnall and B. G. Wybourne, J. Chem. Phys. **40**, 3428 (1964).
[29]W. T. Carnall, P. R. Fields, and B. G. Wybourne, J. Chem. Phys. **41**, 2195 (1964).
[30]N. Edelstein and D. Piehler (unpublished).
[31]J. J. Katz, L. R. Morss, and G. T. Seaborg, in *The Chemistry of the Actinide Elements,* 2nd ed., edited by J. J. Katz, G. T. Seaborg, and L. R. Morss (Chapman and Hall, London, 1986), Vol. 2, p. 1156.
[32]J. D. H. Donnay and H. M. Ondik, *Inorganic Compounds, Crystal Data,* Vol. II, 3rd. ed., Natl. Bur. Stand. (U.S. GPO, Washington, D.C., 1973), p. C-104
[33]F. Auzel and O. L. Malta, J. Phys. **44**, 201 (1983).
[34]W. T. Carnall, H. Crosswhite, and H. M. Crosswhite (unpublished).
[35]W. T. Carnall, J. Chem. Phys. **96**, 8713 (1992).